diffusion-fundamentals

The Open-Access Journal for the Basic Principles of Diffusion Theory, Experiment and Application

Effects of Polydispersity on PGSE NMR Coherence Features

Nirbhay N. Yadav and William S. Price

College of Health and Science, University of Western Sydney, Australia

Corresponding author:
William S. Price
College of Health and Science
University of Western Sydney
Locked Bag 1797, Penrith South DC, NSW 1797, Australia
E-Mail: w.price@uws.edu.au

Abstract

Real systems always contain some degree of polydispersity and yet the effects of this real and very important problem have not been studied in great detail in NMR diffusion experiments. The effects of polydispersity become even less clear when we are outside the short gradient pulse (SGP) limit (which we generally are). Here we investigate the effects of polydispersity, in the form of a Gaussian distribution of characteristic distances, on the coherence features of PGSE NMR experiments of a model system. Characteristic pore sizes were determined from the coherence features and compared to characteristic distances determined from Fourier transforms of the second derivative.

Keywords

PGSE; restricted diffusion; diffusion diffraction; polydispersity; feature enhancement.

1. Introduction

Pulsed gradient spin-echo (PGSE) NMR is a powerful tool ideally suited for measuring molecular dynamics in porous systems. PGSE NMR is unique in that it is non-invasive, it can simultaneously study multiple species independently in a mixed sample, and it can probe the internal structure of samples at length scales much smaller than conventional NMR imaging. Consequently, PGSE NMR is routinely used in a wide range of fields and disciplines such as oil exploration [1-3], drug delivery systems [4], remediation of contaminated waste-water [5,6], and analytical techniques involving chromatographic processes [7-9].

PGSE NMR measures molecular motion via the attenuation of a spin-echo signal. Under certain conditions, diffraction-like effects appear on the echo attenuation curve at regular intervals of the wave vector $\mathbf{q}$ ($=\gamma\delta\mathbf{g}/2\pi$). These coherence features can subsequently be used to probe morphological characteristics of restricted systems (i.e., pore size, tortuosity, and connectivity). For example, polystyrene spheres [10], red blood cells [11], yeast cells [12], brain white matter [12], water-in-oil emulsions [13], and molecules between glass plates [14,15] have been studied using PGSE NMR.

Diffusion Fundamentals 6 (2007) 2.1 - 2.12

Despite the successful characterisation of the systems mentioned above, experimental factors such as background gradients, wall relaxation, and polydispersity can distort or even remove the coherence features in the signal attenuation curve. While bipolar gradients in PGSE pulse sequences have been reasonably successful in removing the effects of background gradients [16-18] and extra terms in the analytical expressions can account for the additional decay due to wall relaxation [19], the mechanisms for dealing with polydispersity have not been investigated in detail.

The systems mentioned above (like all experimental systems) contain some degree of polydispersity (i.e., a distribution of characteristic distances). The subsequent coherence features in polydisperse samples are "damped" because the average weighted signal used in PGSE NMR superimposes nodes at slightly different locations on **q**. In extreme cases the coherence features can completely disappear and the signal attenuation curve may only show Gaussian diffusion and hence may lead to a mis-characterisation of the sample.

Models which assume pores with slanted walls [15,20], a Gaussian distribution of characteristic distances [15], and a combination of smooth and zigzag surfaces [20] have all been fitted successfully to experimental data. Nevertheless, the authors are unaware of any experimental studies which have tested the validity of these models against a range of experimental conditions.

A method for delineating the underlying coherence features in poorly defined PGSE data was proposed by Kuchel et al. [21]. The method involves weighting the data using the Blackman-Harris window function [22], interpolating with a shifting cubic spline, and then the second derivative is taken prior to Fourier transformation. The ability of this numerical tool to identify instances where more than one set of coherence features are present may allow for a more accurate determination of pore structure. Subsequently, the second derivative method can be an important tool for interpreting PGSE diffraction profiles of polydisperse samples.

In this study we use a well defined model system (parallel planes) prepared to give different amounts of polydispersity to test the validity of the Gaussian distribution of characteristic distances model describing polydispersity. Fourier transforms of the second derivative were used in the analysis of the PGSE data.

2. Theory

PGSE NMR spatially labels the position of the spins in a system by recording the phase of the transverse magnetisation via spin-echoes (Fig. 1). The position of the spins is recorded at two instants in time which correspond to two positions (say **r** and **r′**). If **r** and **r′** are identical (i.e., the spins remain stationary or return to their starting position), the net phase change, $\gamma\delta\mathbf{g}\cdot(\mathbf{r} - \mathbf{r}') = 0$, and the spins create a refocussed echo. However, if the spins

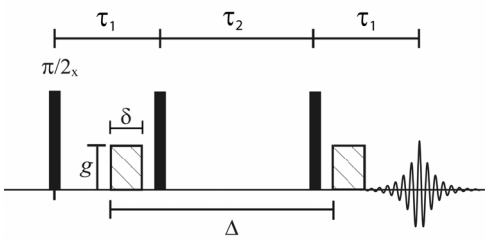

Fig. 1: Schematic representation of the Tanner NMR pulsed field gradient stimulated spin-echo pulse sequence for the PGSE experiment.

move to a different position during the time between the gradient pulses (Δ), $\gamma\delta\mathbf{g}\cdot(\mathbf{r} - \mathbf{r}')$ ≠ 0, their contribution to the echo will be phase shifted. The degree of the dephasing due the applied gradient is proportional to the displacement in the direction of the gradient during Δ. In the case of translational diffusion, each spin in a system will have a random phase change causing the spin-echo signal (Eq. (1)) to attenuate due to averaging of the incoherent phases over the entire sample.

The short gradient pulse (SGP) approximation gives the normalised echo attenuation for a two impulse scheme, such as a Hahn spin-echo based sequence or stimulated spin-echo based sequence (Fig. 1), by [23]

$$E_{\Delta}(\mathbf{g}) = \int \rho(\mathbf{r}) \int P(\mathbf{r} \mid \mathbf{r}', \Delta) \exp\left[i\gamma\delta\mathbf{g} \cdot (\mathbf{r}' - \mathbf{r}) \right] d\mathbf{r}'\, d\mathbf{r} \tag{1}$$

where $\rho(\mathbf{r})$ is the equilibrium spin density and $P(\mathbf{r} \mid \mathbf{r}', \Delta)$, the diffusion propagator, is given by the solution to the diffusion equation. By ensuring $\delta << \Delta$, mathematically tractable equations which describe diffusion within symmetrical pores (e.g., planar [23,24], cylindrical [19,25], and spherical [26,27]) can be derived from Eq. (1). A significant advantage of using the SGP approximation over some other methods is that it can model diffraction-like effects.

Diffraction effects in PGSE NMR derive from the average propagator, which is the probability $\bar{P}(\mathbf{R}, \Delta)$ that a spin at any starting position will displace by **R** during period Δ, is given by

$$\bar{P}(\mathbf{R}, \Delta) = \int \rho(\mathbf{r}) P(\mathbf{r}, \mathbf{r} + \mathbf{R}, \Delta)\, d\mathbf{r} \tag{2}$$

where the diffusion propagator is multiplied by the equilibrium spin density and integrated across the whole sample. In terms of the average propagator Eq. (1) reduces to

$$E(\mathbf{q}, \Delta) = \int \bar{P}(\mathbf{R}, \Delta) e^{i2\pi\mathbf{q}\cdot\mathbf{R}} d\mathbf{R} \tag{3}$$

where **q** is introduced to include the effects of the gradient into the analysis.

In the long time limit (Δ→∞), all species trapped within a pore become independent of their starting positions and, therefore, diffusional processes, so

$$P(\mathbf{r}, \mathbf{r} + R, \infty) = \rho(\mathbf{r} + R)\,. \tag{4}$$

Consequently, the average propagator becomes

$$\bar{P}(\mathbf{R}, \infty) = \int \rho(\mathbf{r}) \rho(\mathbf{r} + \mathbf{R})\, d\mathbf{r}\,. \tag{5}$$

In the limit where the diffusing molecules have sampled the entire pore, the propagator is an autocorrelation function of $\rho(\mathbf{r})$. Using the Wiener-Kintchine theorem [28] and Eq. (3) we find that $E(\mathbf{q}, \infty)$ is the power spectrum of $\rho(\mathbf{r})$,

$$E(\mathbf{q}, \infty) = \left| S(\mathbf{q}) \right|^2 \tag{6}$$

where $S(\mathbf{q})$ is the Fourier transform of $\rho(\mathbf{r}')$.

The signal obtained has no phase information, therefore a Fourier transformation cannot be carried out to obtain structural information from a "conventional" image. Instead, structural information is obtained by plotting the signal attenuation vs. the reciprocal space of acquisition (q). In the case of parallel plane pores,

$$E_{\Delta}(q)=\frac{2\left[1-\cos\left(2\pi\mathbf{q}a\right)\right]}{\left(2\pi\mathbf{q}a\right)^{2}}+4\left(2\pi\mathbf{q}a\right)^{2}\sum_{n=1}^{\infty}\exp\left(\frac{-n^{2}\pi^{2}D\Delta}{a^{2}}\right)\frac{1-\left(-1\right)^{n}\cos\left(2\pi\mathbf{q}a\right)}{\left[\left(2\pi\mathbf{q}a\right)^{2}-\left(n\pi\right)^{2}\right]^{2}} \quad (7)$$

where D the diffusion coefficient and the gradient (**g**) is perpendicular to the planes. The second term in Eq. (7) disappears at long Δ and diffractive minima appear at $\mathbf{q} = n/a$ (n = 1, 2, 3, …) (see Fig. 2).

The accuracy of the SGP approximation is however limited by its reliance on (i) gradient pulses which have durations much shorter than their separations ($\delta << \Delta$), and (ii) the distance diffused during the gradient pulse is small compared to the characteristic dimensions of the system (Eq. (8)),

$$\delta \ll \frac{a^{2}}{D} \quad (8)$$

where δ is the length of the gradient pulse and a is the characteristic distance of the pore. In the case of large molecules in small pores, meeting the condition in Eq. (8) can pose problems for the NMR hardware subsequently leading to errors including an underestimation of the pore size [29,30]. As mentioned earlier, the porous nature of the sample may be lost when these conditions are not met. Subsequently, some authors have developed methods which approximate finite-width gradient pulses by discretising the gradient pulses into intervals of infinitesimally narrow pulses [30,31]. The matrix formalism [30] is particularly successful in significantly reducing errors associated with diffusion during the gradient pulse leading to an underestimation of the pore dimensions and has been experimentally verified [15]. Using this discretisation, the PGSE pulse sequence (Fig. 1) is subdivided into $2N$+1 intervals of length τ such that the total length of the sequence is $(2N+1)\tau$ with

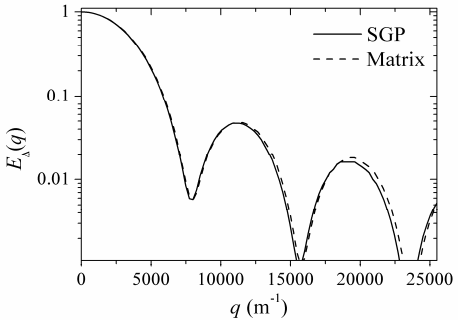

Fig. 2: Simulation of a PGSE coherence feature modelled using the SGP approximation and matrix formalism. Δ was set to 2 s, δ was 2 ms, and the planar separation (a) was 128 μm. The effects of the finite gradient pulses are evident in the matrix-based simulations with the diffractive minima moving to higher **q**.

$$\Delta=\left(N+\frac{1}{2}\right)\tau, \quad (9)$$

$$\delta=\left(M+\frac{1}{2}\right)\tau, \quad (10)$$

hence the total effective scattering wave vector amplitude is

$$q_{\text{net}}=\left(M+1\right)q_{\tau}=\left(M+1\right)\left(2\pi\right)^{-1}\gamma g\tau\ . \quad (11)$$

Finally, the matrix equation for the attenuation is

$$E = S(q)\left[RA(q)\right]^M R^{N-M}\left[RA^\dagger(q)\right]^M RS^\dagger(q) \tag{12}$$

where component matrices are given by

$$\mathbf{S} = \mathbf{B}\mathbf{S}', \tag{13}$$

$$\mathbf{A} = \mathbf{C}^\dagger\mathbf{A}'\mathbf{C}, \tag{14}$$

and

$$R = \exp\left(-k^2\pi^2 D\tau / a^2\right). \tag{15}$$

B and **C** are diagonal matrices defined by

$$\mathbf{B} = \begin{bmatrix} \frac{1}{a} & & & \\ & \frac{\sqrt{2}}{a} & & \\ & & \ddots & \\ & & & \frac{\sqrt{2}}{a} \end{bmatrix}, \tag{16}$$

$$\mathbf{C} = \begin{bmatrix} \sqrt{\frac{1}{a}} & & & \\ & \sqrt{\frac{2}{a}} & & \\ & & \ddots & \\ & & & \sqrt{\frac{2}{a}} \end{bmatrix}, \tag{17}$$

$$S'_k = \begin{cases} \dfrac{i2a\exp(i\pi\mathbf{q}a)(2\pi\mathbf{q}a)\cos(\pi\mathbf{q}a)}{(2\pi\mathbf{q}a)^2 - (k\pi)^2} & k \text{ odd} \\ \dfrac{2a\exp(i\pi\mathbf{q}a)(2\pi\mathbf{q}a)\sin(\pi\mathbf{q}a)}{(2\pi\mathbf{q}a)^2 - (k\pi)^2} & k \text{ even} \end{cases} \tag{18}$$

and

$$A'_{kk'} = \frac{1}{2}\left[S'_{|k-k'|} + S'_{k+k'}\right]. \tag{19}$$

3. Experimental

The model experimental system used in this study was a single pore with parallel boundaries. A water solution (20% H_2O and 80% D_2O) was placed between the tube and plunger of susceptibility-matched microtubes (BMS-3; Shigemi, Tokyo) with the plunger positioned to give a separation of about 150 μm (*a*) with the bottom of the tube with the gradient direction being perpendicular to the planes (Fig. 3a). The end of the plunger was polished with different grades (FEPA system) of sand paper (600 – 120) to obtain surfaces with different degrees of rugosity. After the plunger was polished with the 120 grade sandpaper it was extremely difficult to achieve a small pore size (due to removal of the taper on the plunger as seen in Fig. 3b) therefore experiments carried out had a characteristic distance of approximately 250 μm. To ensure the polished surface was perpendicular the sides of the plunger, a hole (diameter 4 mm) was drilled in an aluminium block that had been machined with high precision to give perpendicular surfaces. The polishing system used only allowed polishing the end of the plunger and not the plane surface within the tube.

^{1}H NMR experiments were performed at 298 K on a Bruker Avance 500 wb spectrometer equipped with a 5 mm broadband inverse probe equipped with a single (i.e., z) shielded gradient coil connected to a GREAT 3/10 current amplifier. The strength of the gradient was calibrated using the known diffusion coefficient of water whilst the temperature in the NMR probe was calibrated using methanol. The stimulated echo pulse sequence with "rectangular" gradient pulses was used to obtain the characteristic diffusion-diffraction pattern. The tube arrangement gave two resonances: a narrow resonance for water between the planes and a broader resonance from water on the sides of the plunger. The two resonances overlapped at low **q** values and could not be separated without significantly degrading the field homogeneity.

Simulations of PGSE coherence features modelled using the matrix formalism were carried out using Mathcad 13 (Mathsoft, Cambridge, MA) and Fourier transforms of the second derivative were performed in *Mathematica* 5.0.

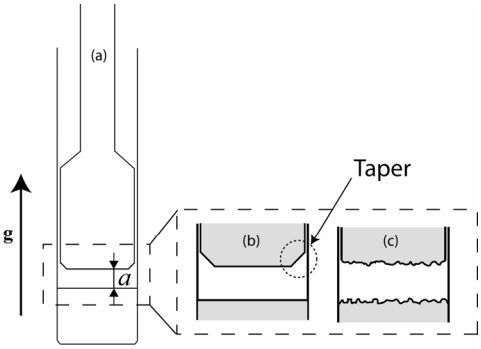

Fig. 3: (a) Shigemi tube arrangement showing the pore of characteristic distance *a* created between the plunger and tube, (b) parallel boundary pore with idealised walls, and (c) parallel boundary pore with rough walls which is approximated by a Gaussian distribution of characteristic distances. The arrow indicates the direction of the magnetic field gradient (**g**).

4. Results and Discussion

Firstly, the rugosity in the parallel pore was modelled using a Gaussian distribution about the spacing in the middle of the tube (a_0) where a weighting factor was introduced to reflect that the NMR signal will be larger from regions of larger separation

$$\rho(z) = \frac{z}{\sigma\sqrt{2\pi}} e^{-\frac{(z-a_0)^2}{2\sigma^2}} \quad [20]$$

where $\rho(z)$ is probability of finding a spin at some value of z and σ is the standard deviation.

The effect of a Gaussian distribution of characteristic distances can clearly be seen in (Fig. 4). A standard deviation of $0.2a_0$ is enough to remove all but the first diffraction minima and a standard deviation of $0.4a_0$ removes all coherence features.

Secondly, the simulations above are supported by experimental data in Fig. 5 where the samples with a higher degree of rugosity clearly show a damping of the coherence features. The absolute attenuation of the experimental data in Fig. 5 is greater than that in the simulations because the free diffusing spins, which attenuate more rapidly, contribute to ^{1}H peak at low qa values. Consequently, the σ values used to damp the modelled diffraction minima and fit the model to the experimental data may be slightly lower than what would be expected if the experimental data only consisted of spins undergoing restricted diffusion.

The shifting of experimental minima to higher qa than the models predict which was seen in previous studies [15] is not observed. Also in Fig. 5a – Fig. 5c, the amount of rugosity in the system was insufficient to decrease the number of maxima/minima cycles in our attenuation curves.

The only other factors which could cause such a damping of the coherence features as seen in Fig. 5 are wall relaxation [24], background gradients [15], and neglecting the motion of spins to adjacent regions with different characteristic dimensions during Δ. Firstly, it has been proven in a number of studies that the surface relaxivity of glass is such that the perfectly reflecting wall approximation is reasonable [15,20,32,33]. Secondly, background gradients still form at the glass-water interface despite using susceptibility matched tubes [34]. Two glass-water interfaces within 100 μm to 300 μm, like those used in this study, result in substantial background gradients which cannot be removed even when using bipolar gradient pulses because the long Δ used enable the spins to travel into regions of different magnetic field strength.

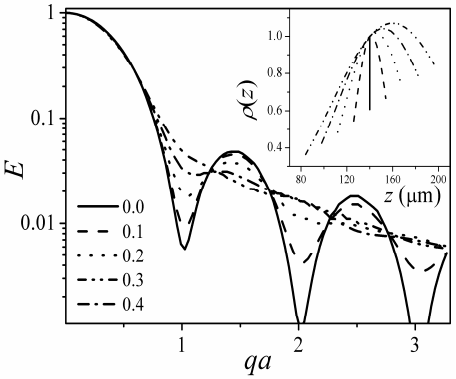

Fig. 4: PGSE coherence data simulated using the matrix formalism of a Gaussian distribution of characteristic distances where σ was varied between $0.0a_0$ to $0.4a_0$. The inset displays the probability of finding a spin at a particular value of z.

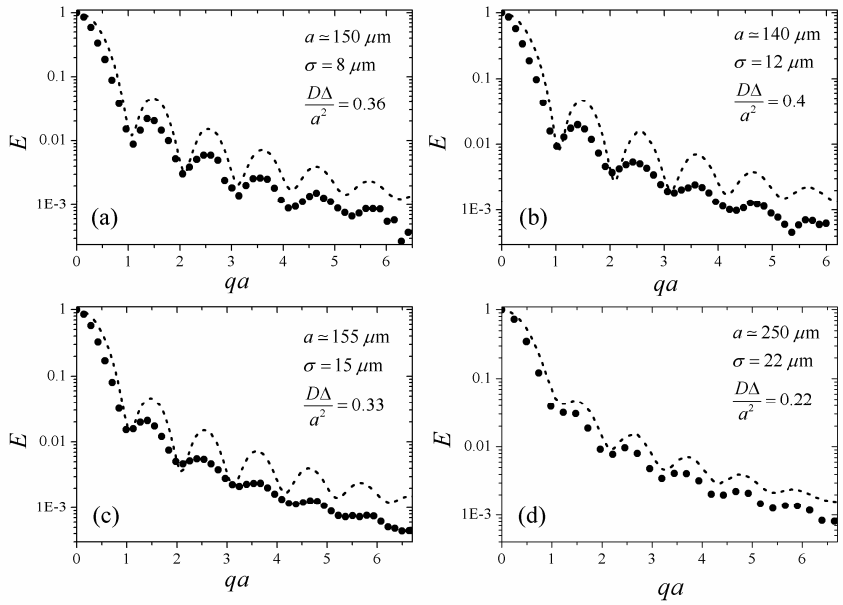

Fig. 5: PGSE signal attenuation profile for water diffusing between planes in a Shigemi tube after (a) no polishing, (b) the plunger polished using 600 grade paper, (c) 400 grade paper, and (d) 120 grade paper. The experimental data in (a-c) was obtained with Δ = 4 s and δ = 2 ms whereas experiments for (d) has Δ = 7 s and δ = 2 ms in order to maintain the $D\Delta/a^2$ ratio. Each spectrum was the average of 32 transients with a recycle delay of typically 36 s which was sufficient to allow for full relaxation (i.e., > 5 x T_1) between each transient. The experimental data was fitted to the model for a Gaussian distribution of characteristic distances (dotted line). The characteristic distances stated on each figure were determined by fitting to the matrix formalism and confirmed using an optical travelling microscope (PTI, Hampshire, England).

Background gradients can be modelled using a cosine profile [35] which has recently been solved [36]. Finally, coherence features only become apparent when a significant portion of the spins sample the boundaries of the confining geometry of a particular characteristic distance. If a spin moves into an adjacent region with a different characteristic distance during Δ, coherence features become less distinct. Pore hopping theory has successfully characterised random walk simulations within regularly spaced rectangular barriers [37] and could be applicable in our model where the interconnection size would approach zero. Presently, the authors are working on more sophisticated models which include background gradients and investigating the applicability of pore hopping models and stochastic boundary conditions.

The probability of finding a spin at each characteristic distance (weighted propagator $P(z)$) was obtained by interpolating the experimental data in Fig. 5, applying the Blackman-Harris window function, taking the second derivative of the interpolations, and finally numerically Fourier transforming the derived data. The weighted propagators in Fig. 6a and Fig. 6c both show characteristic distances very similar to those determined

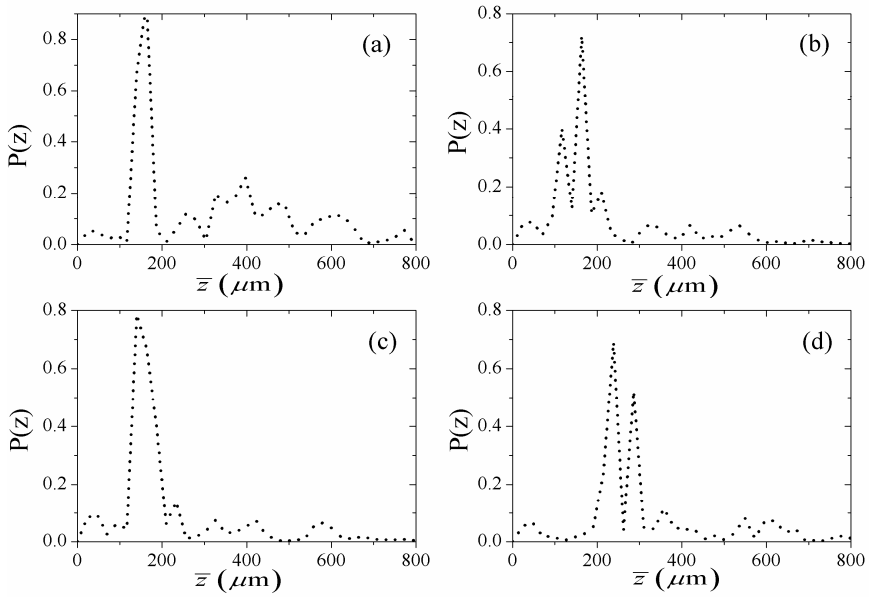

Fig. 6: Weighted propagator P(z) for PGSE NMR q-space data after the application of a Fourier transform of the second derivative. The data in (a) is from a pore of characteristic distance of 150 μm, (b) 165 μm pore after sanding the plunger with 600 grade sandpaper, (c) 140 μm pore after sanding with 400 grade sandpaper, and (d) a 250 μm pore after sanding with 120 grade sandpaper.

directly from the coherence features. The characteristic dimensions determined from Fig. 6b and Fig. 6d are also similar to values determined directly from the coherence features but give two distinct characteristic distances between the parallel planes. Two characteristic distances from samples polished using the 600 and 120 grade sandpaper could explain why there is a misalignment of some nodes from the matrix formalism to nodes in the experimental data.

The potency of the second derivative method for interpreting damped coherence features is further demonstrated in Fig. 7 which contains experimental data and Fourier transforms of the second derivative of the PGSE data obtained from the sample polished using the 120 grade sandpaper at different diffusion intervals (Δ). Even though the coherence features are much less distinct in Fig. 7a compared to Fig. 7b, Fourier transforms of the second derivative gives the same result. Subsequently the second derivative method could be used in more polydisperse systems where the coherence features are less distinct.

The Gaussian distribution model of characteristic distances used in this study was successful in simulating the damping effect of polydispersity but some anomalies exist. For example, the damped coherence features in Fig. 5a also correspond to parallel planes with a wall slanted by 0.4 degrees. For our system a model which incorporates both

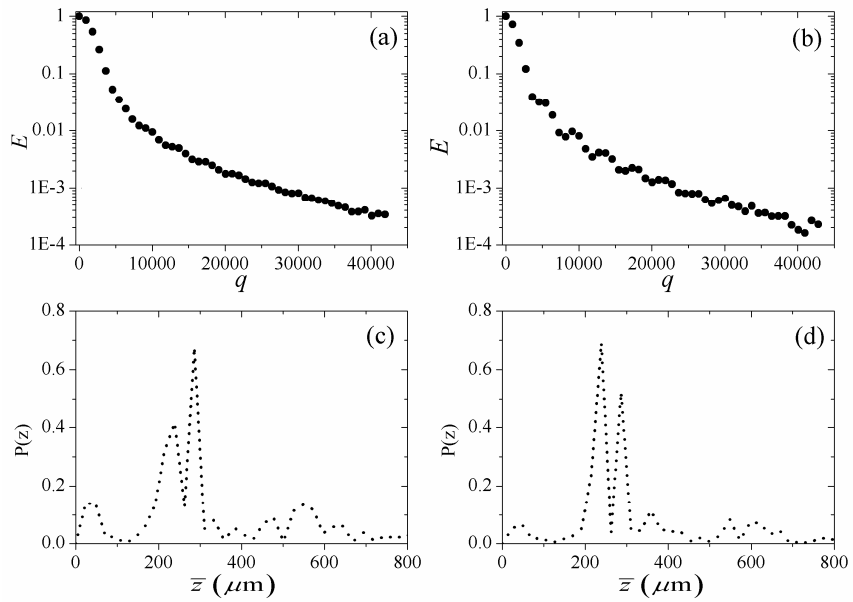

Fig. 7: PGSE attenuation curves (top) and corresponding weighted propagators (bottom) after application of the second derivative method for a pore after sanding with 120 grade sandpaper. The data in (a) and (c) was obtained with $\Delta = 4$ s whist (b) and (d) was obtained with $\Delta = 7$ s. Despite the coherence features in (a) being significantly less distant than those in (b), the weighted propagators give the same characteristic dimensions.

slanted pore walls and a Gaussian distribution of characteristic distances would provide a better fit but will still only be approximations for a stochastic boundary condition.

Given a set of possibly polydisperse PGSE data and with currently available models and methods, one should apply the Fourier transform of the second derivative to determine if there are a few characteristic distances within the sample. Using either the Gaussian distribution of characteristic distances or slanted pore wall models, one can then quantify the polydispersity in the system by fitting the data to simulations of PGSE coherence features using either the matrix formalism or SGP approximation. The authors are currently working on improved techniques for characterising polydisperse PGSE data.

5. Conclusion

The Gaussian distribution of characteristic distances is reasonably successful in describing the polydispersity between parallel planes although a model which considers stochastic boundary conditions would be more ideal. A Fourier transform of the second derivative was however shown to be extremely useful in characterising our model system and explaining possible inconsistencies in experimental results.

6. Acknowledgements

The financial support of the NSW State Government BioFirst award and the UWS postgraduate award is gratefully acknowledged. The authors thank Prof. Philip Kuchel for providing *Mathematica* worksheets on the second derivative method and Mr. Phillip Whitton for his technical support.

References

[1] G. Goelman, and M.G. Prammer, J. Magn. Reson. 113 (1995) 11-18.
[2] W.F. Slijkerman, and J.P. Hofman, Magn. Reson. Imaging 16 (1998) 541-544.
[3] B. Sun, and K.J. Dunn, Magn. Reson. Imaging 23 (2005) 259-262.
[4] S.R. Veith, E. Hughes, and S.E. Pratsinis, J. Control. Release 99 (2004) 315-327.
[5] J. Kärger, and H. Pfeifer, Magn. Reson. Imaging 12 (1994) 235-239.
[6] G.G. Pimenov, and V.D. Skirda, Colloid J. 67 (2005) 746-750.
[7] X.H. Ren, S. Stapf, and B. Blümich, AIChE J. 51 (2005) 392-405.
[8] G. Pages, C. Delaurent, and S. Caldarelli, Angew. Chem. Int. Edit. 45 (2006) 5950-5953.
[9] R. Bujalski, and F.F. Cantwell, Anal. Chem. 78 (2006) 1593-1605.
[10] P.T. Callaghan, A. Coy, D. MacGowan, K.J. Packer, and F.O. Zelaya, Nature 351 (1991) 467-469.
[11] A.M. Torres, R.J. Michniewicz, B.E. Chapman, G.A.R. Young, and P.W. Kuchel, Magn. Reson. Imaging 16 (1998) 423-434.
[12] C. Malmborg, M. Sjobeck, S. Brockstedt, E. Englund, O. Söderman, and D. Topgaard, J. Magn. Reson. 180 (2006) 280-285.
[13] B. Hakansson, R. Pons, and O. Söderman, Magn. Reson. Imaging 16 (1998) 643-646.
[14] W.S. Price, and O. Söderman, Israel J. Chem. 43 (2003) 25-32.
[15] W.S. Price, P. Stilbs, and O. Söderman, J. Magn. Reson. 160 (2003) 139-143.
[16] P.Z. Sun, J.G. Seland, and D. Cory, J. Magn. Reson. 161 (2003) 168-173.
[17] P. Galvosas, F. Stallmach, and J. Kärger, J. Magn. Reson. 166 (2004) 164-173.
[18] J.G. Seland, G.H. Sørland, K. Zick, and B. Hafskjold, J. Magn. Reson. 146 (2000) 14-19.
[19] P.T. Callaghan, J. Magn. Reson. A 113 (1995) 53-59.
[20] D. Topgaard, and O. Söderman, Magn. Reson. Imaging 21 (2003) 69-76.
[21] P.W. Kuchel, T.R. Eykyn, and D.G. Regan, Magnet. Reson. Med. 52 (2004) 907-912.
[22] F.J. Harris, P. IEEE 66 (1978) 51-83.
[23] J.E. Tanner, and E.O. Stejskal, J. Chem. Phys. 49 (1968) 1768-1777.
[24] A. Coy, and P.T. Callaghan, J. Chem. Phys. 101 (1994) 4599-4609.
[25] O. Söderman, and B. Jönsson, J. Magn. Reson. A 117 (1995) 94-97.
[26] J.S. Murday, and R.M. Cotts, J. Chem. Phys. 48 (1968) 4938-4945.
[27] B. Balinov, B. Jönsson, P. Linse, and O. Söderman, J. Magn. Reson. A 104 (1993) 17-25.
[28] D.C. Champeney, Fourier transforms and their physical applications, Academic Press, London ; New York, 1973.
[29] P.P. Mitra, and B.I. Halperin, J. Magn. Reson. A 113 (1995) 94-101.

[30] P.T. Callaghan, J. Magn. Reson. 129 (1997) 74-84.
[31] A. Caprihan, L.Z. Wang, and E. Fukushima, J. Magn. Reson. A 118 (1996) 94-102.
[32] M. Appel, G. Fleischer, D. Geschke, J. Kärger, and M. Winkler, J. Magn. Reson. A 122 (1996) 248-250.
[33] S.L. Codd, and P.T. Callaghan, J. Magn. Reson. 137 (1999) 358-372.
[34] W.S. Price, P. Stilbs, B. Jönsson, and O. Söderman, J. Magn. Reson. 150 (2001) 49-56.
[35] L.J. Zielinski, and P.N. Sen, J. Magn. Reson. 147 (2000) 95-103.
[36] D.S. Grebenkov, J. Chem. Phys. 126 (2007) 104706-104715.
[37] P.T. Callaghan, A. Coy, T.P.J. Halpin, D. MacGowan, K.J. Packer, and F.O. Zelaya, J. Chem. Phys. 97 (1992) 651-662.